K3MnO4: A New Cathode Material for K-Ion Batteries

Armance Sagot, Lorenzo Stievano, Valérie Pralong

K_3MnO_4: a New Cathode Material for K-ion Batteries

Armance Sagot [#,□], *Lorenzo Stievano* [¶,□] *and Valerie Pralong* [#,□,*]

[#,]Normandie University, Ensicaen, Unicaen, CNRS, CRISMAT, 14000 Caen, France

[¶]Institut Charles Gerhardt Montpellier, UMR 5253, CNRS, Université Montpellier, ENSCM, Montpellier 34095, France

[□]Réseau sur le Stockage Electrochimique de l'Énergie (RS2E), FR CNRS 3459, 80039 Amiens, France

AUTHOR INFORMATION

Corresponding Author

* valerie.pralong@cnrs.fr.

Keywords: K-ion Batteries, manganese oxide, cathode, K_3MnO_4, K_2MnO_4

Abstract

In the search for materials used as active species in cathodes for K-ion batteries, only few compositions of transition metal oxides or transition metal polyanionic frameworks have been proposed so far. In this work, we report for the first time the synthesis and study of the electrochemical activity an original K_3MnO_4 polymorph. This phase is a 0D-type structure made of isolated MnO_4 tetrahedra surrounded by K^+ ions. A reversible charge capacity of almost one K^+ per unit formula at the average voltage of 2.3 V vs. K^+/K is obtained, leading to the reversible formation of K_2MnO_4 through a biphasic process.

One of the major challenges of the 21st century is the need to solve the problems related to the management of the energy requested by an ever-increasing consumption, demography and living standards. It is therefore imperative to anticipate this energy demand in a sustainable development context. Storage technologies are highly dependent on the materials used, and it is therefore necessary to search for new advanced materials that are also ecological and cheap. Despite the high performance of lithium-based systems, their production associated with environmental cost is pushing scientists to develop alternative systems based on sodium and potassium, which are abundant and evenly distributed over the Earth's crust. Therefore, in recent years, K-ion batteries (KIBs) have been proposed as a viable alternative. Indeed, this technology has many advantages such as the possibility to use graphite at the negative electrode, aluminum as the current collector and a redox potential of the K^+/K couple of -2.93 V vs. SHE, which could result in a higher energy density than in the case of sodium (-2.71 V), reaching values as high as 150 Wh/kg and 350 Wh/L.[1]

Many cathode materials, belonging to the same families of those already studied for Li-ion and Na-ion batteries (LIBs and NIBs, respectively) have been studied so far.[2,3]. Among them, one could cite vanadium phosphates or Prussian Blue analogues[4] as well as transition metal (TM) oxides including those based on manganese[5]. Regarding the latter family, it is interesting to point out that in the system K-Mn-O, only layered phases with the general formula K_xMnO_2 have been reported as a possible cathode material for KIBs. The layered K_xMnO_2 family was first described by Delmas[6,7] and coworkers, and more recently Kubota[8] and co-workers. Compounds such as P2–

$K_{0.3}MnO_2$ [9] and P3–$K_{0.5}MnO_2$ [10] were reported as efficient cathode materials for KIBs, with reversible capacities of 65 and 100 mAh/g in the potential windows 3.5-1.5 V and 3.9-1.5 V, respectively. However, the layered structure undergoes severe structural distortion and phase transition during K^+ insertion/extraction, resulting in a rapid capacity fading and poor cycling stability. The use of water to expand the interlayer distance for $K_{0.27}Mn_{0.98}O_2$, $0.53H_2O$ produced an improvement in the kinetics of K^+ ion diffusion and in rate capability.[11] However, as reported for Prussian blue analogues,[12] water molecules react at elevated potential[13] conducting to low columbic efficiency[14]. This lack of convincing performance triggered our exploration of alternative KIB cathode materials in the K-Mn-O system.

In this system, a composition attracted our attention: K_3MnO_4. This phase, first reported by Hagenmuller et al.,[15] could be described as a 0D-type structure built of isolated MnO_4 tetrahedra surround by potassium ions. A magnetic study of K_3MnO_4 was performed between 0 and 200 K, proving a paramagnetic behavior and the +V oxidation state of manganese. However, this material has not yet been studied regarding electrochemical potassium (de)insertion. In principle, up to two potassium ions can be removed from the structure, leading to $KMnO_4$ with a theoretical capacity of 227 mAh/g. In addition, we expect also the possible insertion of two potassium ions leading to the composition K_5MnO_4 (171 mAh/g), which does exist in the similar iron-based system (K_5FeO_4).[16] It is also worth noting that in 2007, Saint et al.[17,18] reported the lithium insertion into the phase α-Li_3MnO_4, which is the stable polymorph at low temperature, crystallizing in the wurtzite-type structure.[19,20] This polymorph shows a first discharge capacity of 80 mAh/g corresponding to the insertion of for 0.4 Li in the potential window 4.0-1.8 V.[18] Nevertheless, the capacity drops by 75% after 30 cycles compared to the first discharge value.[21]

Hagenmuller and co-workers succeeded in preparing the two polymorphs of K_3MnO_4 as single crystals by solid-state route from K_2O and MnO_2 under different atmosphere. The high temperature polymorph γ-K_3MnO_4 (obtained at 1100°C under O_2) has a cubic symmetry (P213) with a disordered distribution of K and Mn in similar tetrahedral sites. The low temperature polymorph β-K_3MnO_4, can be prepared by annealing γ-K_3MnO_4 at 300°C under argon. This polymorph has a tetragonal symmetry (I-42m) with ordered MnO_4 tetrahedra. The manganese is reported at the edge and the center of the tetragonal mesh, every manganese is surrounded by four oxygen.

In this work, K_3MnO_4 was prepared via a simple conventional solid-state method starting from of a 10 % excess of potassium superoxide KO_2 (Acros Organic) and manganese oxide MnO (Sigma-Aldrich, 99%), following the chemical reaction: $3KO_2 + MnO \rightarrow K_3MnO_4 + O_2$. The required precursors were mixed together for 2 hours in a planetary ball mill and further heated at 500°C for 12 h in an alumina crucible under vacuum, producing a well-crystallized air sensitive blue colored compound (Fig.1 c)). Note that such color is common for manganese +V oxides.[22] SEM analysis shows large particles of about 10 µm in size (Fig.1 d)) without a particular shape. The corresponding X-ray powder diffraction (XRD) pattern was refined starting from the published cell parameters of the iron analogue K_3FeO_4 (Fig.1 a)),[23] indicating the formation of a previously unknown K_3MnO_4 polymorph. We propose to label this new polymorph α-K_3MnO_4. This phase crystallizes in the orthorhombic space group Pnma with the following cell parameters: a=7.754(1) Å, b=8.960(1) Å, c=7.918(1) Å and a volume of V = 550.998(1) $Å^3$. For this polymorph, [MnO_4] tetrahedra are organized differently compared to the two other known polymorphs. As for the tetragonal structure, they are ordered but alternatively pointing to opposite directions ("zig-zag" arrangement) (Fig. 1b)).

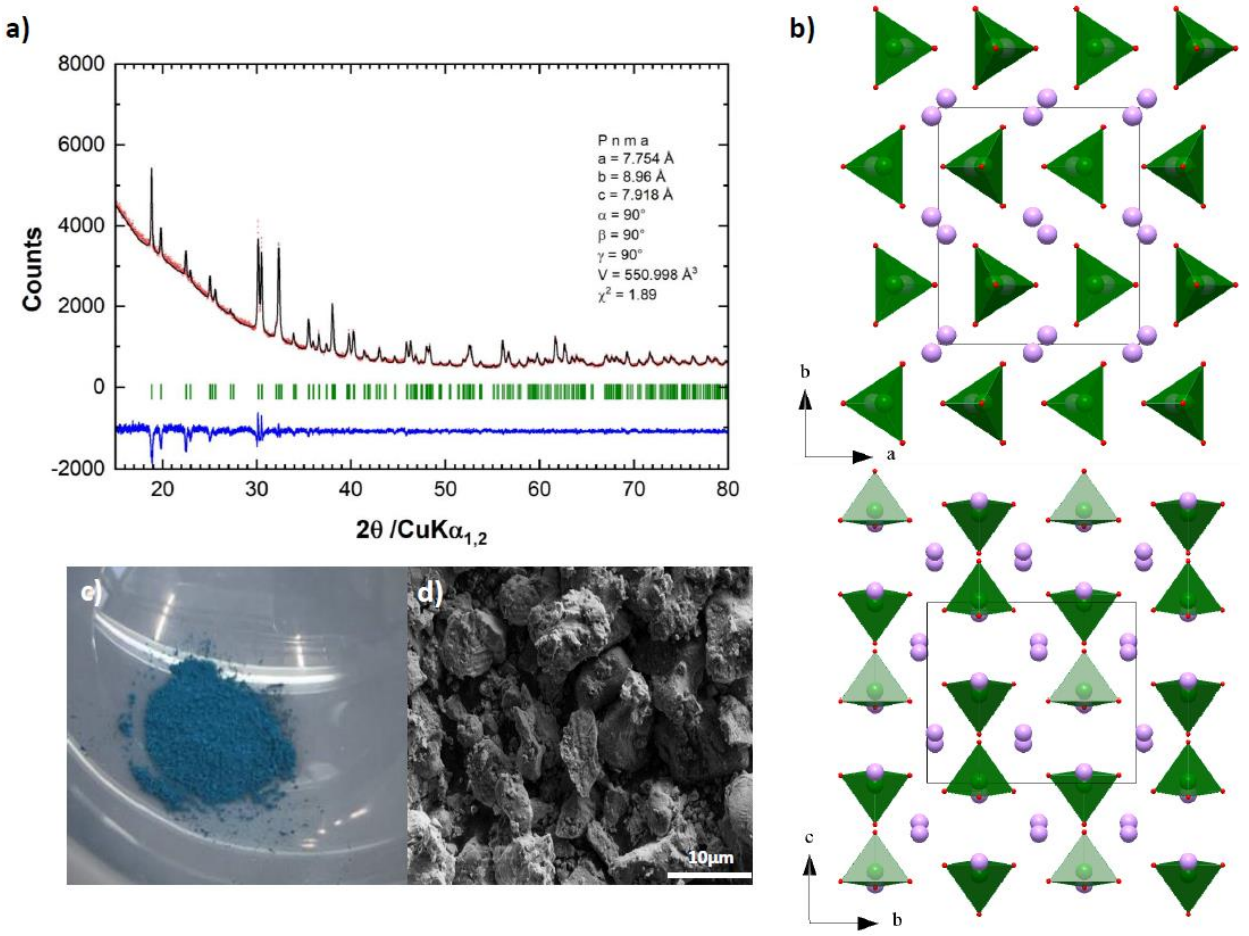

Figure 1 - (a) Rietveld refinement of as-prepared α-K_3MnO_4: experimental (○) and calculated (line) XRD pattern. The difference between experimental and calculated patterns, $y_{obs}-y_{cal}$ is shown at the bottom. (b) α-K_3MnO_4 crystal structure following (001) and (100) axes; (c) Picture and (d) SEM image of as-prepared α-K_3MnO_4.

The charge-discharge profiles of α-K_3MnO_4 were measured by incremental galvanostatic cycling at C/20 (corresponding to the (de)insertion 1 K^+ per unit formula in 20 h) in the potential window 1.6–3.5 V versus K^+/K (Fig. 2a). Despite our attempts, we never succeeded in inserting potassium ions into the structure, probably due to the large size of K^+ ions. Thus, starting from K_3MnO_4, one K^+ could be removed during the oxidation process at 2.6 V vs. K^+/K, leading to the formation of K_2MnO_4. The potentiostatic intermittent titration (PITT) curve shown in Fig.2c reveals a dominant bell shape-type response at 2.66 V, which characterizes a biphasic process, and a second similar but shorter process located at 2.8 V vs. K^+/K. The first biphasic process is also clearly observed (Fig.2 b)) in the derivative curve showing half width length narrower than 50 mV (6 mV on charge

and 28mV on discharge), suggesting the formation of a new phase at the end of the oxidation with a composition close to K_2MnO_4 [24].

As shown on the incremental galvanostatic curve, once the charge is extended above 3.1 V, the process is no longer reversible. A second irreversible phenomenon is observed and may be due to either the further oxidation of Mn, to an anionic redox process or electrolyte decomposition.

On discharge, a reduction plateau at 2.2 V vs K^+/K is observed, corresponding to the insertion of 0.7 K^+ per unit formula. This process, which corresponds to the first oxidation plateau, is reversible upon further cycling, and correspond to a capacity of 70 mAh/g with a Coulombic efficiency of 97.3%. The large polarization of about 400 mV observed between charge and discharge is probably due to the large size of the particles (10 µm diameter).

The rate capacities of the synthesized material are shown in Fig. 2d, the charge capacity was taken at 3.1V ensuring our work in the reversible window potential of 1.6V – 3.1V. The plot of charge capacity indicate is reaching 70 mAh/g after 5 cycles for a C/20 rate. A slight increase in capacity is observed at higher rate, around 75 mAh/g at C/50 and 90 mAh/g at C/100. Nevertheless, it would be necessary to optimize the particle size to increase the capacity.

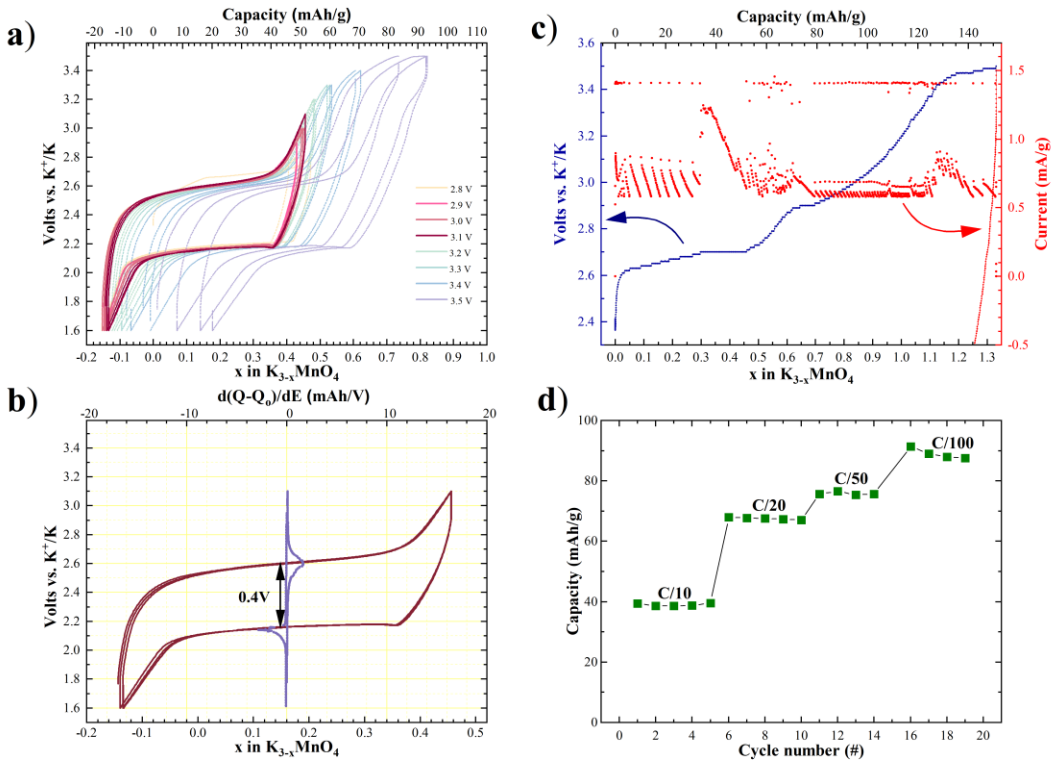

Figure 2. Electrochemical behavior of α-K_3MnO_4. (a) Incremental voltage vs. composition curves for K_3MnO_4 at C/20 rate in the potential window 3.5V-1.6 V; (b) First galvanostatic curve at C/20 in the potential window 1.6-3.1V vs K^+/K and corresponding derivative curves $|dQ/dE|$ versus voltage; (c) PITT curve during the first cycle of K_3MnO_4 in the range of 3.5-2.4 V vs. K^+/K using 5 mV steps for 1 hour and current limitation equivalent to a galvanic current $I_{limit} = I_{C/20}$; (d) and rate capability for the charge capacity at 3.1V versus cycle number.

To have a better insight on the structural changes occurring in the course of the electrochemical process, *operando* XRD patterns were recorded for two full cycles, the first one with limiting the oxidation potential to 3.1 V to highlight the reversibility of the first redox plateau, and the second up to 3.5 V to follow the irreversible process at higher potential (Fig. 3). For the first charge, 0.92 K^+ per unit formula could be deinserted, corresponding to a capacity of 70.4 mAh/g. In the diffraction pattern, the typical diffraction pattern of K_2MnO_4 is observed, in addition to some remaining K_3MnO_4. During this experiment, only 0.92 K^+ per unit formula could be inserted in the following discharge. However, only the XRD peaks of K_3MnO_4 are visible at the end of the discharge, indicating the full reversibility of the process.

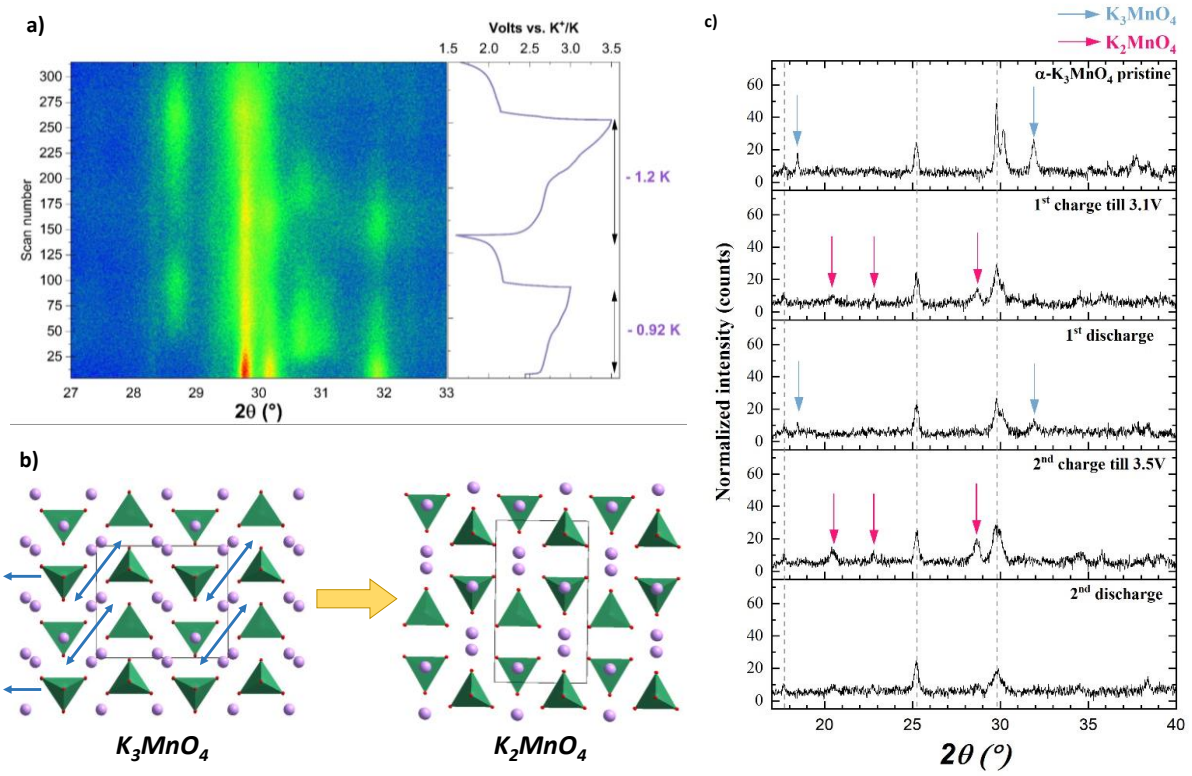

Figure 3. Structural evolution of α-K_3MnO_4 upon potassium ion extraction-insertion. (a) operando XRD analysis during the two first charge-discharge process in a K half-cell at a current rate of C/20 between 1.6-3V for the first cycle and 1.6V-3.5V vs K^+/K for the second cycle. XRD patterns were collected every hour, corresponding to an exchange of 0.05 K^+ per pattern. (b) Structural view along the c axis of orthorhombic K_3MnO_4 and K_2MnO_4. (c) XRD powder patterns of α-K_3MnO_4 during operando measurement after the different charge and discharged. Reflection attributable to K_3MnO_4 and K_2MnO_4 phase are indicated with blue and red arrows, respectively. Dotted lines correspond to the common peaks between the two phases.

For the second charge, 1.2 K^+ ions per unit formula could be deinserted, corresponding to a capacity of 93.7 mAh/g. During the whole *operando* measurement, a decrease in intensity and a broadening of the diffraction peaks is observed, indicating the gradual decrease in crystallinity of the different phases. However, while K_2MnO_4 peaks (20.45°, 22.72° and 28.66°) are observed at the end of both first and second charge, those of K_3MnO_4 (18.49° and 31.97°) are not recovered at the end of the second discharge, indicating the total and irreversible amorphization of the material

during oxidation above 3.5V vs K^+/K. Nevertheless, the low signal-to-noise ratio of the *operando* XRD patterns makes it difficult to fully characterize the structure of these materials, and synchrotron XRD, possibly combined with neutron diffraction should be performed to better characterize the structure of these phases, in particular that of the intermediate phase that seems to form half-way through the first and second charge (Figure 3 a). Given the paramagnetic nature of K_3MnO_4, a study of its magnetic properties was carried out as well as that of the fully oxidized one obtained at 3.5 V vs. K^+/K. From the dependence of the magnetization on the temperature, one can estimate the manganese oxidation state using the Curie-Weiss law. For the pristine material, (without carbon black), an average manganese oxidation state of +4.4 is obtained. After one charge up to 3.5 V, the oxidation state of Mn is +5.8, very close to Mn^{+VI}, which would correspond to the formation of K_2MnO_4.

In conclusion, these results confirm the deinsertion of one K^+ per unit formula from the new polymorph α-K_3MnO_4 through a biphasic phenomenon at 2.66 V, which accompanies the oxidation of manganese from Mn^{+V} to Mn^{+VI}. This oxidation goes along with a decrease of the cell volume by 15% between K_3MnO_4 and K_2MnO_4. This process corresponds to a reversible capacity of 70 mAh/g at C/20 with a relatively large polarization (400 mV), which can in principle be improved by optimizing the electrode formulation and the particle size of the material. Above this potential, the further extraction of K^+ gives rise to an irreversible process, which corresponds to a progressive amorphization of the system. It is important to underline that this material, non-toxic and inexpensive, is in addition very easy to prepare. This finding confirms the interest of the exploration of the K–Mn–O system for the discovery of alternative electrode materials for KIBs.

EXPERIMENTAL METHOD

The compounds were characterized by XRD using a SMARTLAB (Rigaku) diffractometer with Bragg-Brentano geometry ($CuK_{\alpha 1,2}$ radiation). Note that due to their instability in air, XRD patterns were registered using 0.4 mm diameter quartz capillary. The *operando* XRD measurement was carried out on a MiniFlex (Rigaku) diffractometer with Bragg-Brentano geometry ($CuK_{\alpha 1,2}$ radiation). For the electrochemistry measurement, a SP-50 potentiostat (Biologic SA, Claix, France) couple with electrochemical cell with a Berylium window was used.

Operando analyses were performed with an homemade cell described in a previous paper.[25] In this study, a beryllium window is used, a cathode material of about 15 mg was made with K_3MnO_4 (70 wt%) PTFE (10wt%) and black carbon (20w%). The material was cycled at C/20 and XRD scans were continuously measured between 5° and 50°. Each XRD scan had a duration of about 10 min. A scanning electron microscope (SEM) Zeiss Field Effect Gun (FEG) XL-30 with a resolution of about 1 nm was used to study the sample morphology, while the elemental compositions were confirmed by energy dispersive spectroscopy (EDS) on a Link-Isis analyzer (ATW 6650 detector). Magnetic measurements were carried out with a SQUID magnetometer (MPMS, Quantum Design). For each sample the zero-field-cooled (ZFC) and field-cooled (FC) data were collected with an applied field of 1000 Oe. The magnetic susceptibility was calculated by dividing the magnetization by the magnetic field value. The field-dependent magnetic moment values were collected at 5 K. The Curie–Weiss fitting $\chi = \frac{N_A \mu_\beta^2 \left(\mu_{eff}^2\right)}{3kT}$ of the χ (T) curve for 250K < T < 350K yields to calculated effective paramagnetic moment with $\mu_B = 9.274.10^{-24}$ erg/G, k = $1.381.10^{-16}$ erg/K, $N_A = 6.022.10^{23}$ $mol^{-.1}$ and the $\mu_{eff}^2 = 2 * \sqrt{S(S+1)}$ [26]. The experimental effective magnetic moment for the two composition were $\mu_{eff}(K_3MnO_4)$ = 3.5μB and $\mu_{eff}(K_2MnO_4)$ = 2.63μB. The electrochemical characterization was performed in Swagelok-type cells with a solution 0.8M KPF_6 in EC:DEC as the electrolyte and metallic potassium as the counter-electrode. The working electrode was prepared from a mixture of K_3MnO_4 with acetylene black in a weight ratio of 50:50. The electrochemical cells were cycled at constant current between 1.6-3.5 V on a BCS potentiostat/galvanostat (Biologic SA, Claix, France) at room temperature. Potentiostatic intermittent titration technique (PITT) measurements were conducted using potential steps of 5 mV limited by a mini-mum current equivalent to a C/100 galvanostatic rate.

AUTHOR INFORMATION

Armance Sagot : armance.sagot@ensicaen.fr, https://orcid.org/0009-0001-1839-973

Valerie Pralong : valerie.pralong@ensicaen.fr, https://orcid.org/0000-0003-4644-8006 https://www.valerie-pralong.cnrs.fr, @ValeriePralong,

Lorenzo Stievano: lorenzo.stievano@umontpellier.fr, https://orcid.org/0000-0001-8548-0231, @loroik

Notes

"The authors declare no competing financial interest."

ACKNOWLEDGMENT

The authors thank J. Jean, G. Riou, S. Gascoin, S. Duffourt and L. Hervé for technical help. Financial support from the French National Research Agency (project Labex STORE-EX, ANR-10-LABX-76-01) as well as from the Intercarnot Project #252156 "CaKi - Cathode Materials for K-ion Batteries" (Carnot Institutes EPS and CBC) is gratefully acknowledged.

REFERENCES

(1) Yan, Z.; Obrovac, M. N. Quantifying the Cost Effectiveness of Non-Aqueous Potassium-Ion Batteries. *J. Power Sources* **2020**, *464*, 228228. https://doi.org/10.1016/j.jpowsour.2020.228228.

(2) Eftekhari, A. Potassium Secondary Cell Based on Prussian Blue Cathode. *J. Power Sources* **2004**, *126* (1–2), 221–228. https://doi.org/10.1016/j.jpowsour.2003.08.007.

(3) Eftekhari, A.; Jian, Z.; Ji, X. Potassium Secondary Batteries. *ACS Appl. Mater. Interfaces* **2017**, *9* (5), 4404–4419. https://doi.org/10.1021/acsami.6b07989.

(4) Li, A.; Duan, L.; Liao, J.; Sun, J.; Man, Y.; Zhou, X. Formation of Mn–Ni Prussian Blue Analogue Spheres as a Superior Cathode Material for Potassium-Ion Batteries. *ACS Appl. Energy Mater.* **2022**, *5* (9), 11789–11796. https://doi.org/10.1021/acsaem.2c02288.

(5) Duan, L.; Xu, J.; Xu, Y.; Tian, R.; Sun, Y.; Zhu, C.; Mo, X.; Zhou, X. Cocoon-Shaped P3-Type K0.5Mn0.7Ni0.3O2 as an Advanced Cathode Material for Potassium-Ion Batteries. *J. Energy Chem.* **2023**, *76*, 332–338. https://doi.org/10.1016/j.jechem.2022.10.006.

(6) Delmas, C.; Fouassier, C. Les Phases KxMnO2 (x < 1). *Z. Fur Anorg. Allg. Chem.* **1976**, *420* (2), 184–192. https://doi.org/10.1002/zaac.19764200211.

(7) Delmas, C.; Fouassier, C.; Hagenmuller, P. Evolution cristallochimique et propriétés physiques de quelques oxydes lamellaires. *Mater. Sci. Eng.* **1977**, *31*, 297–301. https://doi.org/10.1016/0025-5416(77)90049-0.

(8) Kubota, K.; Dahbi, M.; Hosaka, T.; Kumakura, S.; Komaba, S. Towards K-Ion and Na-Ion Batteries as "Beyond Li-Ion." *Chem Rec* **2018**, *18* (1), 22. https://doi.org/10.1002/tcr.201700057.

(9) Vaalma, C.; Giffin, G.; Buchholz, D.; Passerini, S. Non-Aqueous K-Ion Battery Based on Layered K0.3MnO2 and Hard Carbon/Carbon Black. **2016**. https://doi.org/10.1149/2.0921607JES.

(10) Kim, H.; Seo, D.; Kim, J. C.; Bo, S.; Liu, L.; Shi, T.; Ceder, G. Investigation of Potassium Storage in Layered P3-Type K $_{0.5}$ MnO $_{2}$ Cathode. *Adv. Mater.* **2017**, *29* (37), 1702480. https://doi.org/10.1002/adma.201702480.
(11) Gao, A.; Li, M.; Guo, N.; Qiu, D.; Li, Y.; Wang, S.; Lu, X.; Wang, F.; Yang, R. K-Birnessite Electrode Obtained by Ion Exchange for Potassium-Ion Batteries: Insight into the Concerted Ionic Diffusion and K Storage Mechanism. *Adv. Energy Mater.* **2019**, *9* (1), 1802739. https://doi.org/10.1002/aenm.201802739.
(12) Potassium-Ion Batteries: Key to Future Large-Scale Energy Storage? **2020**, 15.
(13) Hurlbutt, K.; Wheeler, S.; Capone, I.; Pasta, M. Prussian Blue Analogs as Battery Materials. *Joule* **2018**, *2* (10), 1950–1960. https://doi.org/10.1016/j.joule.2018.07.017.
(14) Lu, Y.; Wang, L.; Cheng, J.; B. Goodenough, J. Prussian Blue: A New Framework of Electrode Materials for Sodium Batteries. *Chem. Commun.* **2012**, *48* (52), 6544–6546. https://doi.org/10.1039/C2CC31777J.
(15) Olazcuaga, R.; Reau, J.-M.; Leflem, G.; Hagenmuller, P. Préparation, Proprietés Cristallographiques et Magnétiques des Phases K3XO4 (X=V, Cr, Mn). *Z. Fur Anorg. Allg. Chem.* **1975**, *412* (3), 271–280. https://doi.org/10.1002/zaac.19754120311.
(16) Frisch, G.; Rohr, C. K5FeO4 und K17Fe5O16 : Zwei neue Kalium-Oxoferrate(III). 7.
(17) Saint, J. A.; Doeff, M. M.; Reed, J. Synthesis and Electrochemistry of Li3MnO4: Mn in the +5 Oxidation State. *J. Power Sources* **2007**, *172* (1), 189–197. https://doi.org/10.1016/j.jpowsour.2007.07.027.
(18) Yu, Z.; Xie, S.; Liu, X.; Cui, Y.; Liu, H. Electrochemical Evaluation of Li3MnO4 Used as Cathode Materials for Lithium-Ion Batteries. *Solid State Ion.* **2012**, 72–78. https://doi.org/10.1142/9789814415040_0009.
(19) Meyer, H.; Hoppe, R. Zum thermischen Verhalten von Li3MnO4 I. [1]. Über α- und β-Li3MnO4. *Z. Für Anorg. Allg. Chem.* **1976**, *424* (3), 249–256. https://doi.org/10.1002/zaac.19764240308.
(20) Kilroy, W. P.; Dallek, S.; Zaykoski, J. Synthesis and Characterization of Metastable Li–Mn–O Spinels from Mn(V). *J. Power Sources* **2002**, *105* (1), 75–81. https://doi.org/10.1016/S0378-7753(01)00973-9.
(21) Surace, Y.; Simões, M.; Pokrant, S.; Weidenkaff, A. Capacity Fading in Li3MnO4: A Post-Mortem Analysis. *J. Electroanal. Chem.* **2016**, *766*, 44–51. https://doi.org/10.1016/j.jelechem.2016.01.029.
(22) Collins, T. J.; Gordon-Wylie, S. W. A Manganese(V)-Oxo Complex. *J. Am. Chem. Soc.* **1989**, *111* (12), 4511–4513. https://doi.org/10.1021/ja00194a063.
(23) Hoppe, R.; Mader, K. Zur Konstitution von K3[FeO4]. *Z. Fur Anorg. Allg. Chem.* **1990**, *586* (1), 115–124. https://doi.org/10.1002/zaac.19905860116.
(24) Palenik, G. J. Crystal Structure of Potassium Manganate. *Inorg. Chem.* **1967**, *6* (3), 507–511. https://doi.org/10.1021/ic50049a016.
(25) Sottmann, J.; Pralong, V.; Barrier, N.; Martin, C. An Electrochemical Cell for Operando Bench-Top X-Ray Diffraction. *J. Appl. Crystallogr.* **2019**, *52* (2), 485–490. https://doi.org/10.1107/S1600576719000773.
(26) Kittel, C. *Introduction to Solid State Physics*, 8. ed.; Wiley: Hoboken, NJ, 20.

TOC GRAPHICS